MICROMACHINED STIMULATING ELECTRODES

Quarterly Report #8

(Contract NIH-NINDS-N01-NS-2-2379)

July --- September 1994

Submitted to the

Neural Prosthesis Program
National Institute of Neurological Disorders and Stroke
National Institutes of Health

by the

Solid-State Electronics Laboratory
Bioelectrical Sciences Laboratory
Department of Electrical Engineering and Computer Science
University of Michigan
Ann Arbor, Michigan
48109-2122

October 1994

MICROMACHINED STIMULATING ELECTRODES

Summary

During the past quarter, research under this program has focused in several areas. We have continued to produce a variety of passive stimulating probes and provide them to internal and external users. Additional experiments have been performed in penetrating the pia and dura with both single-shank and ten-shank probe structures. Both probes with shallow-diffused (sharp, 10°) tips and probes with deep-diffused (blunt, 45°) tips penetrate the pia mater with little discernable cortical dimpling. The cortical depression using these tips with an insertion rate of 1mm/sec is estimated at about 250μm and 800μm, respectively. The force on the probe shanks is in about the same ratio for these two tip designs. New interface electronics for the on-chip strain gauges now allows ample force resolution, but breathing and cardiovascular artifacts remain a problem. None of these probes have successfully penetrated dura mater since their present thicknesses (14μm) reduce their stiffness and allow them to buckle excessively before penetration. During the coming term we hope to extend these measurements to eliminate some of the artifacts and to explore the effects of insertion rate on force and cortical dimpling. It is noteworthy that using the sharp tips, we see virtually no bleeding even when intentionally penetrating surface blood vessels. The insertion holes are evidently self-sealing, both with the probe in place and when they are removed.

Experiments to evaluate tissue reaction to stimulation continued during the quarter. Using charge-balanced anodic-first 50μA current pulses with 100μsec per phase, anodic bias (0.6V) on the site was found to significantly reduce back-voltage. SEM inspection of sites on a probe implanted and stimulated for five days, and then sacrificed four weeks later, showed tissue adhering to all sites that were stimulated. No site that was inactive (not used for stimulation) had any appreciable tissue growth over it. Most sites that were stimulated had an overlay of tissue on them, sometimes relatively thick in appearance. Tests to further understand and quantify these effects are continuing.

A new computer-controlled system for site activation, deactivation, and cyclic voltammetry is also being developed using LabVIEW. The system will offer the user control over a variety of parameters, will ensure reproducibility in the activation process, and will require minimal user interactions during the activation process. This system is now nearing completion.

We believe the iridium adhesion problems we have been experiencing for the past three years are now understood and can be eliminated from future runs. The problems have been traced primarily to the RIE dielectric etch step which precedes metal deposition. This step has been depositing fluorocarbon films ("teflon") on the sites which acts as an electrical impedance barrier and degrades adhesion of the titanium metal, deposited as a glue under the iridium. Secondarily, moisture is a problem degrading adhesion. We have found that minimization of RIE overetch, increasing the titanium thickness to ensure adequate coverage over all of the site, use of a dehydration bake prior to metallization, and

use of a 500°C 30sec rapid thermal anneal after lift-off can eliminate these adhesion problems.

A new run of active stimulating probes has been completed. A full set of second-generation active probes (STIM-1b, STIM-1a, and STIM-2) has been realized. All of these probes appear to be functioning adequately. More detailed in-vitro and in-vivo tests should begin during the coming quarter.

MICROMACHINED STIMULATING ELECTRODES

1. Introduction

The goal of this research is the development of active multichannel arrays of stimulating electrodes suitable for studies of neural information processing at the cellular level and for a variety of closed-loop neural prostheses. The probes should be able to enter neural tissue with minimal disturbance to the neural networks there and deliver highly-controlled (spatially and temporally) charge waveforms to the tissue on a chronic basis. The probes consist of several thin-film conductors supported on a micromachined silicon substrate and insulated from it and from the surrounding electrolyte by silicon dioxide and silicon nitride dielectric films. The stimulating sites are activated iridium, defined photolithographically using a lift-off process. Passive probes having a variety of site sizes and shank configurations have been fabricated successfully and distributed to a number of research organizations nationally for evaluation in many different research preparations. For chronic use, the biggest problem associated with these passive probes concerns their leads, which must interface the probe to the outside world. Even using silicon-substrate ribbon cables, the number of allowable interconnects is necessarily limited, and yet a great many stimulating sites are ultimately desirable in order to achieve high spatial localization of the stimulus currents.

The integration of signal processing electronics on the rear of the probe substrate (creating an "active" probe) allows the use of serial digital input data which can be demultiplexed onto the probe to provide access to a large number of stimulating sites. Our goal in this area of the program has been to develop a family of active probes capable of chronic implantation in tissue. For such probes, the digital input data must be translated on the probe into per-channel current amplitudes which are then applied to the tissue through the sites. Such probes require five external leads, virtually independent of the number of sites used. As discussed in our previous reports, we are now developing a series of three active probes containing CMOS signal processing electronics. Two of these probes are slightly redesigned versions of an earlier first-generation set of designs and are designated as STIM-1A and STIM-1B. The third probe, STIM-2, is a second-generation version of our high-end first-generation design, STIM-1. All three probes provide 8-bit resolution in setting the per-channel current amplitudes. STIM-1A and -1B offer a biphasic range using $\pm$5V supplies from 0μA to $\pm$254μA with a resolution of 2μA, while STIM-2 has a range from 0 to $\pm$127μA with a resolution of 1μA. STIM-2 offers the ability to select 8 of 64 electrode sites and to drive these sites independently and in parallel, while -1A allows only 2 of 16 sites to be active at a time (bipolar operation). STIM-1B is a monopolar probe, which allows the user to guide an externally-provided current to any one of 16 sites as selected by the digital input address. The high-end STIM-2 contains provisions for numerous saftey checks and for features such as remote impedance testing in addition to its normal operating modes. It also offers the option of being able to record from any one of the selected sites in addition to stimulation.

During the past quarter, research on this contract has focused in several areas. We have measured the insertion forces as a function of tip shape in pia arachnoid and have found the sharp shallow-diffused tips enter tissue with significantly less cortical dimpling and force than do their larger double-diffused counterparts. Additional work was also done on the characterization of stimulating sites in-vivo. Anodic electrode bias helps to minimize electrode impedance, and there is a clear indication that tissue overgrowth on sites is a

function of site stimulation. A new electrode characterization system for site activation is under development and is nearing completion. Finally, we have completed a new run of active stimulating probes. The etching problems experienced with a previous run were corrected and the probes appear fully functional in all respects. They will be tested with the full computer interface in-vitro and then in-vivo during the coming quarter. The results in each of these areas are described below.

2. *Penetration Studies with Passive Stimulating Probes*

The penetration studies have been described in previous reports with regard to the design of the different probe geometries that were fabricated and tested. In brief, a set of passive probes was designed and fabricated incorporating different designs for the tip and shank geometries in order to study the tissue coupling, insertion forces, and tissue damage associated with inserting the probes through the pia arachnoid of guinea pigs and other experimental animals. The probes and associated data acquisition system were designed to collect data that would help to define the optimum probe shank geometry: one that provides the best combination of low penetration force, minimal cortical dimpling, minimal tissue damage and/or reaction along the insertion track, and maximum electrode-tissue coupling for stimulation and recording purposes.

The probes incorporate integrated polysilicon strain gauges at the bases of the shanks for measuring penetration force. It was previously reported that difficulty was being experienced in recording these strain gauge signals because the signal was getting lost in the noise of the data acquisition system (a Mac IIfx with LabVIEW running with a National Instruments I/O board, described in detail in a previous report). During the past quarter, a circuit was designed and built for amplifying the strain gauge signal immediately after coming off the probe. The circuit consists of a classical Wheatstone bridge and a custom bioinstrumentation amplifier with a level-shifting output stage as shown in Fig. 1. A gain of about 1060 was used to raise the bridge imbalance voltage well above the system noise.

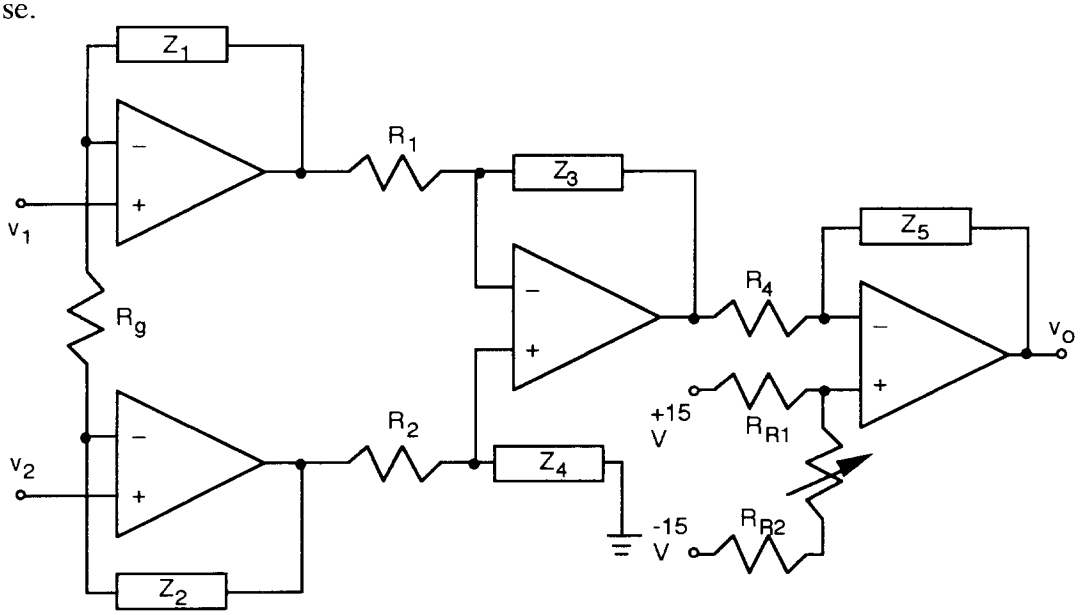

Fig. 1: The bioinstrumentation amplifier configuration used for the penetration-probe strain gauges with a level-shifter on the final stage for zeroing out bridge imbalance due to resistor mismatch.

The circuit uses the probe strain gauge as one leg of the bridge and three discrete resistors hand-picked to match the unstrained resistance of the probe as the other legs (the resistors must be hand-picked for each probe since the resistance varies from probe to probe). A perfect resistor match is impossible, but small offset voltages can be compensated for with the level-shifter in the output stage. This feature allows the unstrained resistance to be set to zero volts output. This also makes possible full utilization of the ±10 volt input range of the analog-to-digital converter on the data acquisition board. Because of the high gain and low input signal level, special attention had to be given to shielding the circuit and probe from external noise. With this in mind, the entire amplifier circuit, the bridge, and the probe mounting 'stalk' were enclosed in an aluminum case which was directly mounted on the microdrive. The three resistors and the probe stalk were socket mounted to make it easy to change them. Only the end of the stalk, with the mounted probe, remained unshielded, since it extended out through a hole in the aluminum case. The amplifier was also designed as a low-pass filter with a bandwidth of less than 100Hz. This cutoff frequency was intended to provide prefiltering prior to sampling at 200Hz. The low sampling frequency was determined by the rate at which the computer could synchronously request and acquire position and voltage data from the microdrive controller board and the I/O board, respectively. The careful attention to noise shielding and filtering paid off, and a noise level of approximately 5mV$_{p-p}$ output was realized. This means that a 10μV bridge imbalance voltage will still be seen, being twice as large as the system noise.

With the new amplifier circuit in place in the data acquisition system, the output of the probe strain gauges had to be calibrated. A probe was advanced against a rigid object while continuously recording position and strain gauge output as seen in Fig. 2. The relationship between tip deflection and output is not linear because of the nonlinearity introduced by having only one strain gauge in the bridge instead of a complementary pair. As it turns out, the output during penetration into pia arachnoid never exceeds 1.5V, which corresponds to only about 1μm of tip deflection. Over that range, the output can be approximated as a linear function of tip deflection as shown in Fig. 3. Once this relationship (volts per μm of axial tip tip deflection) was known, the axial force could be calculated from a numerically derived solution to the column buckling problem which relates tip deflection to the axially-applied force. This mechanical theory was discussed in the previous report.

Penetrations were performed in guinea pig with single-shank probes at a velocity of 1mm/sec. An attempt was made to penetrate dura mater, with the same negative results as reported earlier. It was not possible to penetrate the dura with either blunt (deep boron-diffused) or sharp (shallow boron-diffused) probes. The pia arachnoid was easily penetrated by both types of tips (the PSA4565-DB (deep boron diffused, 45° tip angle) and the PSA1065-SB (shallow boron diffused, 10° tip angle). The penetration data for both tips are shown in Fig. 4 for comparison. The difference in ease of penetration is seen in the different output voltage amplitudes from the respective strain gauges. The reduction for the sharper tip is approximately a factor of three. The differences in cortical dimpling are demonstrated by the narrower range of microdrive displacement (from cortical contact to penetration) for the sharper tip. Again, dimpling is reduced by about a factor of three. Unfortunately, all of the penetrations did not produce good results as can be seen in Figs. 5 and 6, which are plots of PSA4565-DB and PSA1065-SB penetrations, respectively. The sharp probe in general demonstrated worse artifacts than did the more rounded probe. The reason for this greater artifact sensitivity has not yet been determined. The probes are very sensitive to the slightest movement of the probe tip. Present in these traces are what we believe to be artifacts due to brain pulsation with respiration and heart rate as well as possible temperature sensitivity of the probe strain gauge. This temperature sensitivity was expected since all of the resistors of the bridge circuit are not on the probe substrate. The

output of the circuit has a tendency to drift slowly due to changing temperature. We tried to minimize temperature effects by having the tip of the probe bathed in the CSF prior to penetration in an attempt to bring the probe substrate up to near body temperature. This would help keep the strain gauge from experiencing a significant temperature swing during penetration. We are currently trying to correlate the different features of these signals (i.e., the large slow rise and fall and the smaller more rapid jumps) to different possible sources. Breathing and heart rate artifacts could be eliminated by euthanizing the animal and then performing the penetrations; however, it has been observed that the surface of the brain gets tacky very quickly after euthanization. This has the effect of making the brain cling to the probe shanks more, increasing the dimpling and adding a new complexity to an already complex situation.

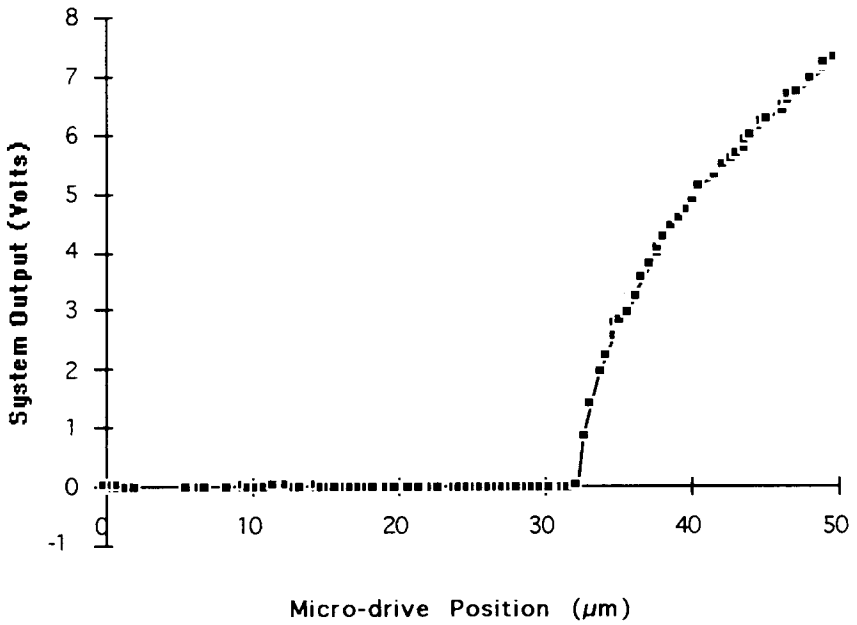

Fig. 2: Relationship between system output voltage and probe deflection.

A battery of penetrations was performed with six different 2D multishank probes (the shallow-boron and deep-boron versions of arrays having 200μm shank spacings, 400μm shank spacings, and an array with 200μm shank spacings and tapered shank lengths, the center tine being the longest). The penetrations were recorded on video tape. Each of the arrays was advanced at different speeds (100μm/sec, 1mm/sec, and 5mm/sec) into the cortex of a guinea pig through intact pia arachnoid; the dimpling and ease of penetration were observed. The purpose of these penetrations was to get a qualitative feel for the differences between the different shank configurations. From visual observation, it appeared that higher insertion speeds and sharper tips performed better, as expected. They produced less cortical dimpling. However, it was unclear if there was an advantage in having an array with the shanks tapered, at least with the center shanks being the longest. It appeared that this geometry may, in fact, result in greater dimpling. This could be possible in that as the center shanks depressed the cortex and were approaching penetration force, the adjacent shanks suddenly made contact and began to depress the cortex even further, thus slowing the rate of force buildup on the more central shanks. The result is a more global and severe dimpling of the cortical surface. In the case of the non-tapered shanks, the pressure appeared to be distributed evenly over the central shanks while

building up on the end shanks. The end shanks have a load-sharing shank on only one side; therefore, they penetrate first. Upon penetration, the end shank no longer supports the pressure of the pia arachnoid and the next shank in effect becomes the end shank. Once started, the penetrations progress inward quite rapidly, almost like a domino effect. If these observations are correct, it could be due to our selecting the wrong initial taper. This could be corrected by making the next shank short enough so as not to touch the cortex until its neighbor has already achieved penetration.

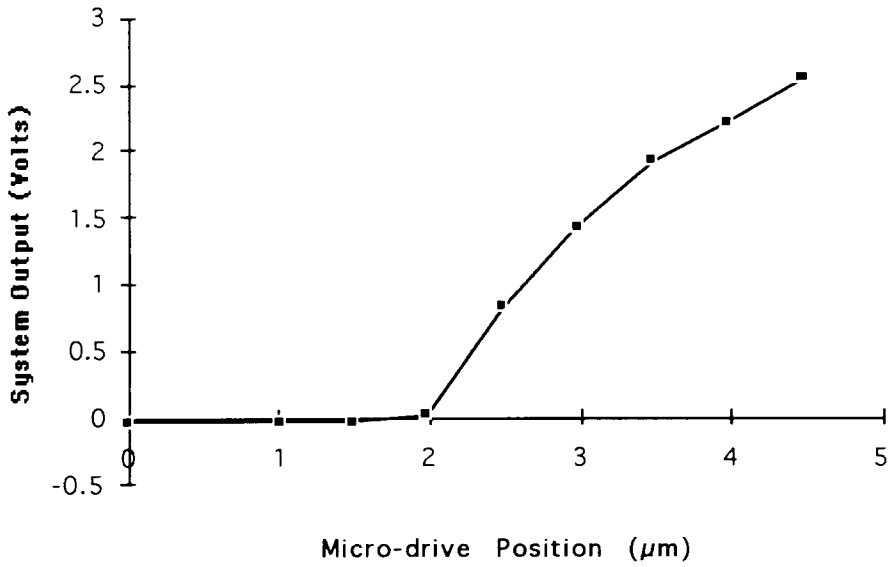

Fig. 3: Relationship between system output and the microdrive position (probe deflection) in the normal range of operation.

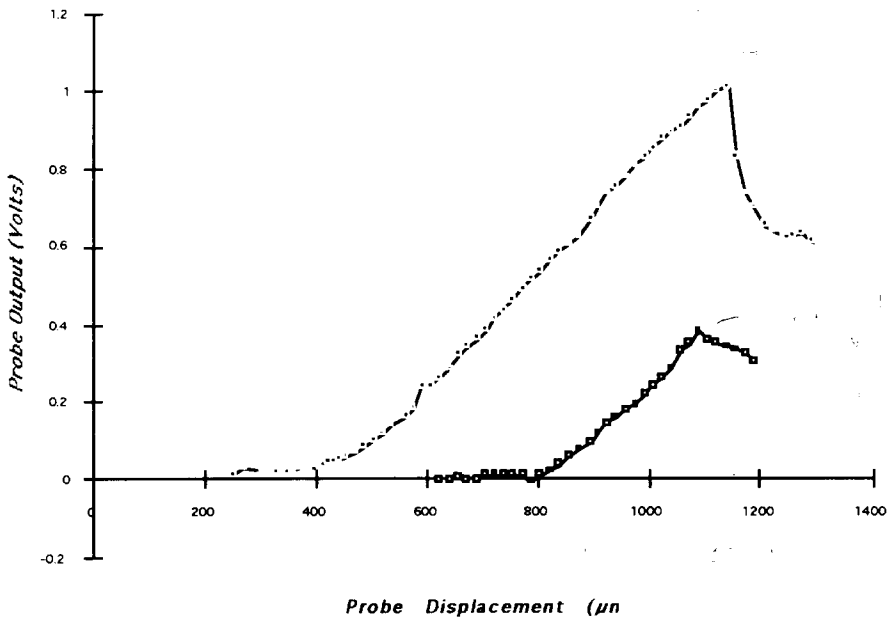

Fig. 4: Penetrations with both a PSA1065-SB (shallow boron diffused, 10° tip angle) probe and a PSA4565-DB (deep boron diffused, 45° tip angle) probe, demonstrating the differences in penetration force and cortical dimpling.

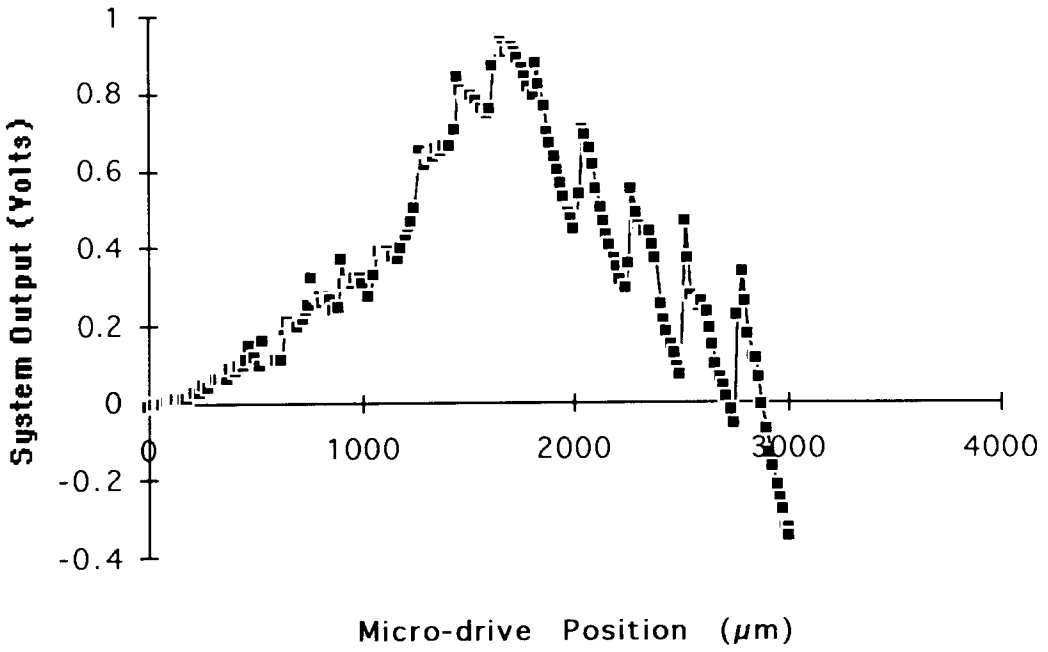

Fig. 5: Penetration with a PSA1065-SB (shallow boron diffused, 10° tip angle) probe, which demonstrates the large amount of artifact that can hide the penetration signal.

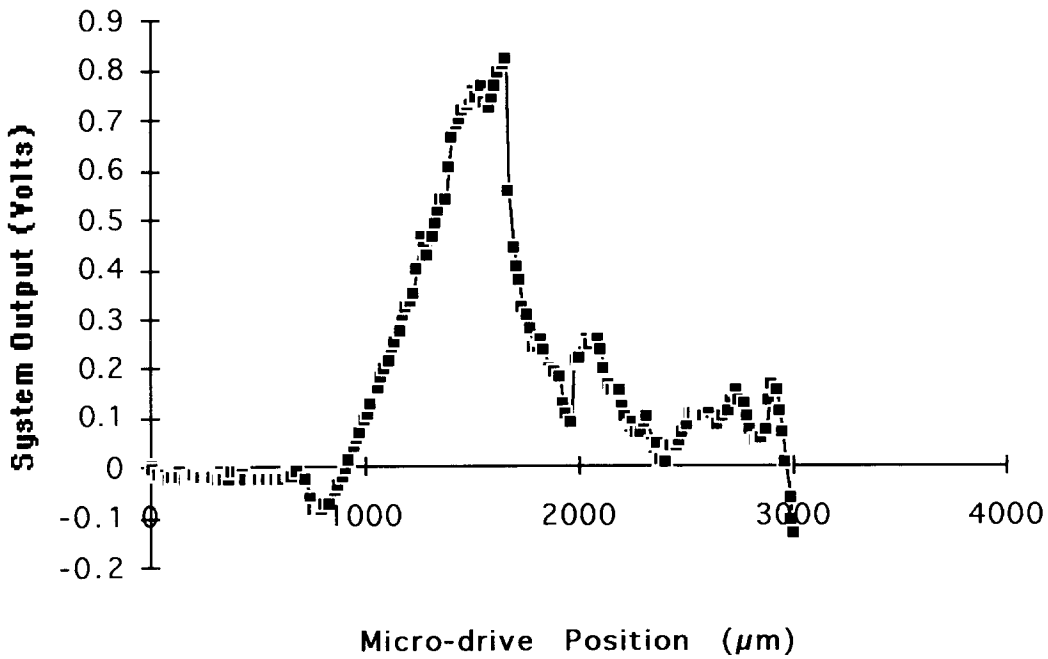

Fig. 6: Penetration with a PSA4565-DB (deep boron diffused, 45° tip angle) probe, which demonstrates the reduced artifact typically present.

Several penetrations were also made through blood vessels in the cortex. It was observed that sharp tips could penetrate a blood vessel and be removed with little or no observable hemorrhaging from the puncture. The same could not be said for the blunt tip; in fact, several times punctures resulted in significant hemorrhaging.

When the data collection techniques are perfected for a single shank, the amplifier circuit will be replicated to make it possible to simultaneously record from all three of the strain gauges on the 2D arrays. This will give further insight into the distribution of penetration forces and cortical dimpling across the array. It should also help in understanding how a tapered shank configuration performs in comparison to a non-tapered probe.

During the coming quarter, we hope to solve the problem of acquiring clean penetration data by singling out and eliminating or otherwise minimizing the effects of the various artifacts. It is expected that we will be able to rule out or, if necessary, clean up any temperature related effects. Penetration experiments will be performed as a function of insertion speed. We also anticipate proceeding with the artificial neuron experiment in both acute and chronic situations. This will give us further insight into the falloff in recorded signal amplitudes with time during chronic implants of passive probes.

3. *In-Vivo Current Flow and Impedance Studies*

This past quarter*in vitro* and *in vivo* experiments were performed showing the effects of a voltage bias on stimulating sites. Also, SEM photos were taken of a chronically implanted probe after its removal from the preparation.

The chronic stimulation experiments run this quarter were similar to those reported previously and will be reviewed briefly. A passive, three-shank stimulating electrode was used. Each shank carries a pair of 1000μm^2 sites. The sites were activated to 30mC/cm^2. In-vitro tests were run in phophate-buffered saline. For in-vivo tests, the electrode was placed in the right occipital lobe of an adult guinea pig. A recovery period of 7-10 days postop followed. Two site pairs on an electrode were both stimulated for four hours each on five consecutive days. One of the site pairs was placed at a 0.6V bias during stimulation (as discussed below). The stimulation waveform consisted of two biphasic pulses, 100μs per phase. The leading pulse was anodic, followed 1ms later by a cathodic pulse. This waveform was presented at 500Hz. The current magnitude was 50μA. The voltage drop across the site pair was recorded in response to the above waveform and to a 1kHz sine wave (for gain and phase measurements). Records were saved at the beginning and end of the four hour period and at 30 minute intervals during the stimulation.

Bias Effects

Others have reported a significant decrease in back voltage when an activated iridium site is biased at a small positive voltage (0.6V vs. SCE). This method has been incorporated into our stimulation protocol. The results are shown below both *in vitro* (Figs. 7 and 8) and *in vivo* (Figs. 9 and 10).

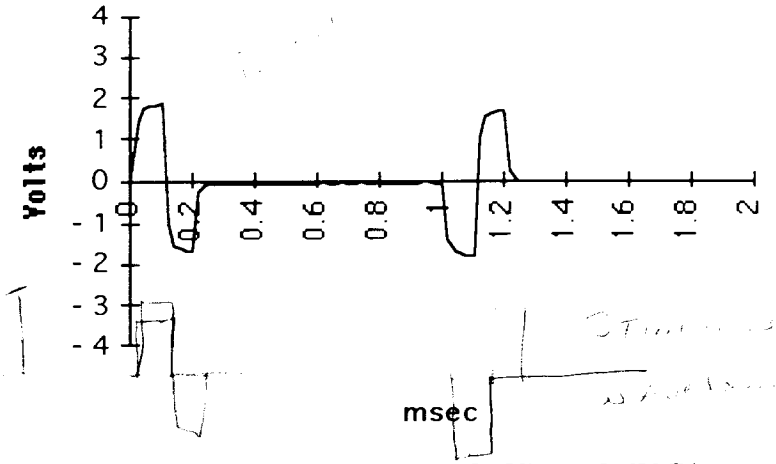

Fig. 7: Bipolar Voltage Drop, *In Vitro*, 0.6V Bias

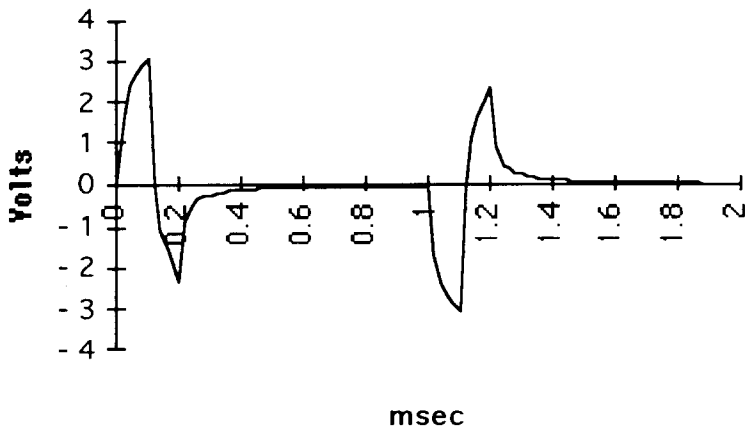

Fig. 8: Bipolar Voltage Drop, *In Vitro*, No Bias

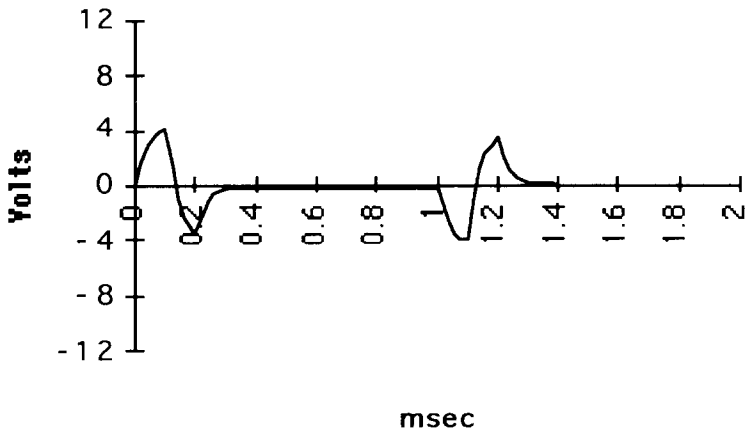

Fig. 9: Bipolar Voltage Drop, *In Vivo*, 0.6V Bias

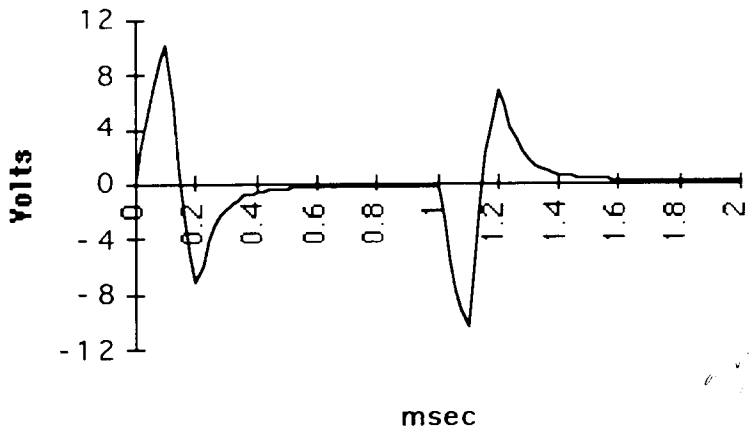

Fig. 10: Bipolar Voltage Drop, *In Vivo*, No Bias

The results of these two experiments suggest that the iridium oxide maintained its electrical characteristics for the *in vitro* test but not the *in vivo* test. Recall that the electrode is being stimulated using a bipolar waveform. Therefore, when one site is anodic, the other is cathodic. This means that if both sites are anodically biased, then one site will have to go additionally positive on the leading pulse. Such a voltage excursion may violate the water window and, consequently, damage the oxide. The oxide appeared in electrical tests to be stable for the *in vitro* test. Cyclic voltammetry (CV) tests were run prior to a stimulation period. The results indicated that the oxide was not affected by the bias (i.e., charge density was fairly constant). Also, the back voltage remained unchanged for the entire week for both the biased and unbiased sites. However, the *in vivo* test showed a back voltage that was not stable. This has been seen previously without biasing (see the last report) so we are unsure of the source of this variability. Possible causes include poor quality oxide or poor metal adhesion. Additional instrumentation is being developed to run the CV tests in vivo. This capability will help us determine the state of the oxide at various times over the experimental period. Also of concern is the effect biasing has on nearby neural tissue. Future experiments will involve recording evoked responses to electrical stimuli in the auditory system. Examination of this chronic data should give some indication of the condition of the neurons close to the sites and their response to biasing.

Photos of an electrode that had been chronically implanted were obtained using a SEM (ISI DS-130). The probe shown in the figures below had 1000μm^2 sites and had been used in a chronic stimulation experiment. The experimental protocol was identical to that described above with a current magnitude of 50μA. The animal was sacrificed 4 weeks after the completion of stimulation. The tissue was fixed in 4% periformaldehyde prior to dissection. The photos below show one site that had been used for stimulation (Fig. 11) and one that was inactive (Fig. 12). The active site shows tissue growth similar to that reported last quarter. The unused site also has a thin coating, but it does not appear to be directly related to the presence of the site (it extends along the shank as well). Two other active sites were also examined. No material was present on these sites. Summarizing the observations, not every active site has selective tissue growth, but no inactive site has such tissue growth. We are developing a experiment to determine the nature of the material on the site.

Fig. 11: SEM photograph of an iridium oxide stimulating site that was used for stimulation in-vivo according to the protocol noted in the text. There is significant material growth on the site.

Fig. 12: SEM photograph of an iridium oxide stimulating site that was implanted in-vivo but not used for stimulation. The site is relatively free of material.

4. A Software-Controlled Site Activation Station

During the past quarter, work continued on setting up an automated test station to grow anodically formed iridium oxide films (AIROFs) on the stimulating sites of multielectrode probe arrays. This test station is needed because the present system is outdated. In addition, this station will provide more flexibility than the present system by allowing multiple sites to be processed without continual user interaction. This will allow up to sixteen sites on a multielectrode probe array to be activated overnight. The station will be capable of performing electrode site activation, deactivation, and cyclic voltammetry (CV). A block diagram of the station is shown in Fig. 13. It was hoped that the station would be completed this past quarter, but it is not. The hardware implementation and testing required more time than anticipated.

Significant progress was made last quarter. The station software, including the user interface and the process control for each function, is written and only requires modifications to more accurately calculate the electrode charge capacity. The buffering, amplifying, and filtering circuits have been designed and implemented. They will be modified only if necessary to improve the accuracy of the electrode charge capacity calculation. The switching circuit used to select a particular site has been designed and its functionality demonstrated, but it requires further testing with the other circuitry. In addition, a method for suspending the probe arrays in solution and connecting them to the circuit has been designed and implemented. The system is currently cleaning and activating electrodes and providing current-voltage graphs of cyclic voltammetry tests. However, there are a few areas that require more development. First, a more accurate calculation of the electrode charge capacity is needed to determine when activation should cease as well as to provide this information to the user after each CV test. Also, the site switching circuitry needs to be fully integrated into the other circuitry. In addition, a problem has been observed where the chronic probe floats to the surface of the solution during the cleaning process. This floating is caused by bubbles that form on the electrode surface during the cleaning process. Because the electrode is not immersed in solution for the entire cleaning process, the oxide layer is not completely removed from the electrode. A permanent solution to this problem is being investigated. Lastly, a method for packaging the system electronics in a permanent housing must be selected and implemented. All of these areas will be addressed in the next quarter.

5. Studies of Iridium Adhesion

During the past few years of neural probe development, we have increasingly been plagued by poor metal adhesion in connection with our iridium sites. The problem has slowly gotten worse over the past three years in spite of detailed studies of iridium sputtering conditions and other process parameters. The iridium, which is under high compressive stress as deposited, will simply buckle and pop off of the substrate, creating bubbles of local lifting in metallization or coming off the substrate completely. This problem has destroyed more fabrication runs in the last year than have been successful, magnifying the work of making probes by a factor of three or more. In addition to these adhesion problems, we have also noticed a barrier film present at many of our contacts. This film is evident as a higher-than-normal impedance between the interconnect material and the site that can be broken down by passing current through the site at voltages of a few volts or less; however, recording sites and polysilicon gate leads never see such voltage across them, further complicating the problem. Thus, many of our recent recording electrodes have been defective and our yield of active recording probes has also been low.

We have decreased our iridium thickness from 3000Å to 1500Å or less during the past two years in hopes that this would decrease the stress and help the adhesion problem, but without noticeable success. The problem tends to be quite intermittent and random, even on a given wafer, making definitive studies more difficult. During the past quarter, in some desperation, we did a detailed study of these problems and have come to an understanding of their causes. As had been suspected, the "barrier film" and the adhesion problem are really two manifestations of the same problem, and it is not an iridium adhesion problem but rather a titanium-to-oxide/polysilicon adhesion problem. This is remarkable, since titanium is extremely reactive and is known to adhere quite well to these materials.

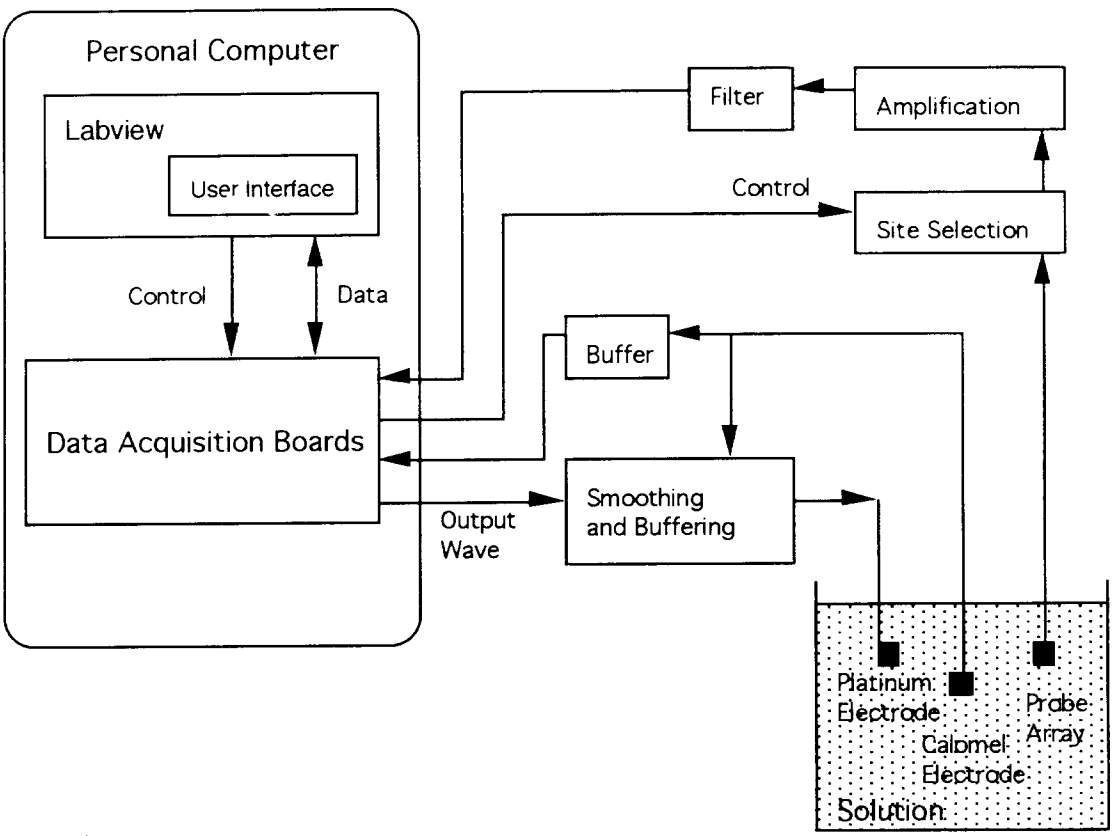

Fig. 12: Block diagram showing the new test station that will be capable of activating multiple sites without continual user interaction.

Figure 13 shows the structure of one of our typical sites. The triple layer combination of stress-relieved dielectrics (oxide-nitride-oxide) is opened over the intended site using a CF_4 etch in the RIE with a photoresist mask. In order to try to remove all oxide present, the wafers are deliberately overetched up to 50% longer than required in the RIE and are then given a short buffered HF etch to remove any residual oxide, rinsed in deionized water, spun dry, and taken directly to the sputtering chamber to be pumped down. With the same resist still in place, the titanium and then the iridium are deposited. The wafers are then removed from the sputtering chamber and the photoresist is removed, lifting off the metal from over the field areas but retaining it where the photoresist had been removed over the sites and pads to allow the metal to adhere to the substrate. This sequence is especially effective with small sites since it self-aligns the metal to the contact

opening (they use the same photoresist layer as mask). Unfortunately, by overetching the contacts in RIE and then moving quickly from the water rinse to the sputtering chamber, we were doing exactly the wrong things from the standpoint of metal adhesion.

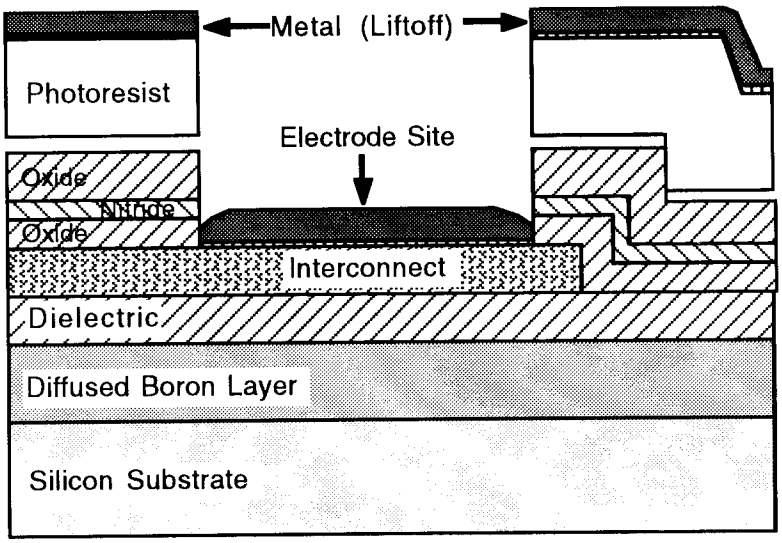

Fig. 13: Formation of an electrode site structure for the neural probes.

Causes of Poor Adhesion

As a result of studies during the past quarter, the following sources of poor metal adhesion have been identified:

1. Fluorocarbon (FC) Film Formation during RIE

Some researchers have reported that a FC layer can be formed by means of plasma deposition via the polymerization of carbonhydrotrifluoride (CHF_3). The properties of these FC films are comparable to those of polytetrafluoroethylene (PTFE), better known under the trademark names of Teflon and Fluon. Their properties include high resistivity ($10^{16}\Omega$-cm), chemical inertness, high fracture strains (300-500%), a low surface free energy, and a low coefficient of friction. Fluorocarbon (FC) films are commonly used as passivation layers, as insulating layers, as antisticking layers, or as layers for the reduction of friction.

The recipe for etching oxide in our RIE (CHF_3=25sccm, CH_4=25sccm, 40mT, 185W) contains the gas CHF_3; therefore, it is highly possible to form a FC layer through polymerization due to the reaction of the photoresist, the chemical gases, and the products of the RIE oxide etch during the etching of site contact openings. We believe this to be the primary source of our adhesion problems. We have inadvertently been putting teflon down under our metal. And overetching to be particularly careful was exactly the wrong thing to do. The more the overetch, the thicker the FC film.

2. Reduced Adhesion due to Residual Moisture

Prior to sputtering the site metal, the wafers are normally subjected to a 30sec BHF dip followed by a 3min DI H_2O rinse. The wafers are then dried in a spin dryer. Incomplete drying at this step can allow moisture to remain in the contacts, which can cause poor metal adhesion.

3. Thin Metal (Ti or Cr) at Site Corners due to Shadowing

The metal "glue" layer used under the noble site metal is used to promote adhesion between the bottom interconnect layer and the upper metal film. During these metal tests, the deposition profile of the metal after sputtering was observed to be very nonuniform due to the rather steep edges on the etched sites (about 3-4μm high including the photoresist). For example, the thickness of the metal film near the contact edges is only about 30-40% of that in the center region for 10μm wide patterns as shown in Fig. 14. This is due to shadowing of the bottom of the site openings by the sidewalls. This deposition ratio (edge vs. center thickness) is dependent on the site profile; that is, higher aspect ratio (height vs. width) patterns have greater non-uniformity. Therefore, if the target metal thickness is too low (e.g., Ti or Cr, 300-500Å thick), the metal may not be thick enough at the edges to act as a satisfactory glue layer for the top metals (Au or Ir). This can lead to lifting around the edges of the site.

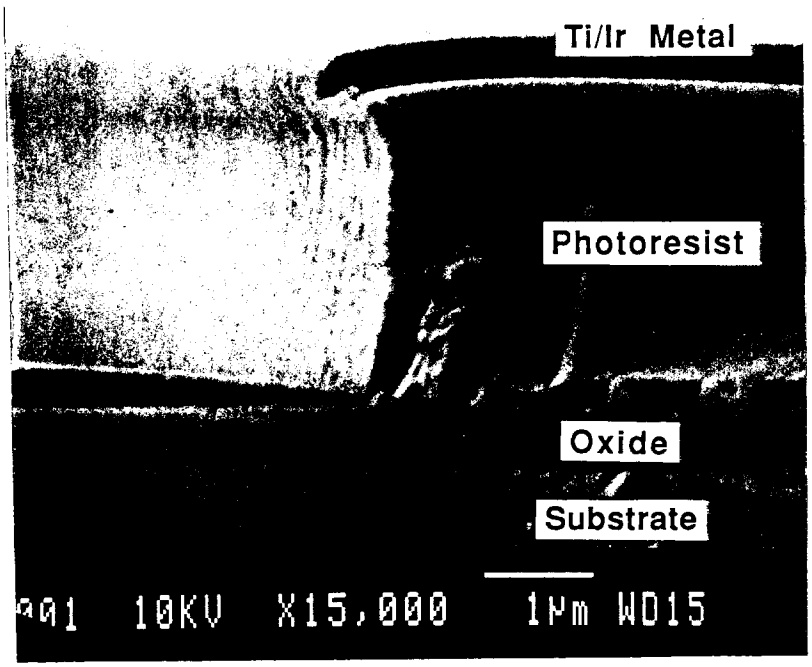

Fig. 14: Metal profiles for 10μm wide patterns. The shadowing effect can be seen at the edges of the site along the bottom.

Experimental Results

1. Single Layer Tests (silicon, oxide, polysilicon)

The single layer tests were performed to identify which of these layers might cause poor metal adhesion. A group of wafers was divided into three subgroups: bare silicon,

silicon dioxide (including several types of oxide: thermal, LTO, LPCVD, PECVD), and polysilicon in order to test metal adhesion to each material. Each of these groups were divided and half were patterned with photoresist so that lift-off could be performed. These subgroups were again divided and sputtered with Cr/Au or Ti/Ir (500Å/3000Å in Ar=30sccm, 7mT ambient) for these tests. Note that the iridium thickness is back at 3000Å for all of these tests and that we are sputtering at pressures consistent with high stress and high charge capacity.

Initial visual inspections did not reveal any adhesion problems on any of these materials. Scratch tests, performed with a wafer scriber, showed that the adhesion was, in fact, very good (no tearing or "bubbling up" was seen along the scratches; the metal only smears out). It should be noted that these scratches are a severe adhesion test and score through the metal film, the underlying dielectrics, and into the silicon. From this test we concluded that the processing parameters related to only single layers are not the factors responsible for poor metal adhesion. That is, if the metal films are deposited onto silicon, silicon dioxide, or polysilicon directly, there are no adhesion problems whether the metal is used with a lift-off process or the metal is just deposited everywhere on the underlying substrate. Figure 15 shows examples of scratch tests performed with Ti/Ir on a thermal oxide layer sample.

2. Multilayer Tests including RIE (overetch of 10% vs. 50%)

We now prepared samples that had structures similar to that of the passive probe sites. The samples were divided into two groups, and the sites were opened using RIE, the first group of samples being overetched by 10% and the second group by 50%. The etch rate of the thin film layers (oxide, nitride, and polysilicon) is normally characterized every months in our laboratory to provide known etch rates for RIE users. This etch rate was used in conjunction with the measured oxide film thickness to determine the target etch time. After the contacts were opened, the metal was sputtered as usual, and a lift-off process was performed to pattern the metal. The test results revealed far more than we expected. Inspection of the 50% overetched samples revealed that some of the site metal patterns were flaking off. The 10% overetched samples appeared to have good adhesion. Inspection after the scratch tests, however, revealed that the metal bubbled up (tore away) around the scratches for both the 10% and the 50% overetched samples. The 50% overetched samples had much worse adhesion problems than the 10% overetched samples. This difference may be due to the formation of a thicker FC layer during the longer dry etch. Figure 16 shows patterns on a 50% overetched sample after lift-off; nearly all of the patterns here have buckled even without scratching. Figure 17 shows the results for 10% overetched patterns. Here the unscratched patterns look fine, but when scratched they buckle free of the substrate, indicating poor adhesion. We have seen all of these conditions on probe wafers over the last three years, sometimes in abundance.

3. Wet vs. Dry Sample Tests

"Wet" and "dry" samples were prepared for sputtering to see if moisture had an effect. Wet samples were prepared by the partial removal of water after the BHF rinse; dry samples were baked in an oven for 5min at 110°C after being dried in a spin dryer. The "dry" samples were found to have better adhesion than the "wet" samples but the differences between the wet and dry samples was not as much as was expected. Figure 18 shows samples with a 10% overetch and wet vs. dry processing. In the case of dry processing, very little adhesion difficulties are noted even after scribing.

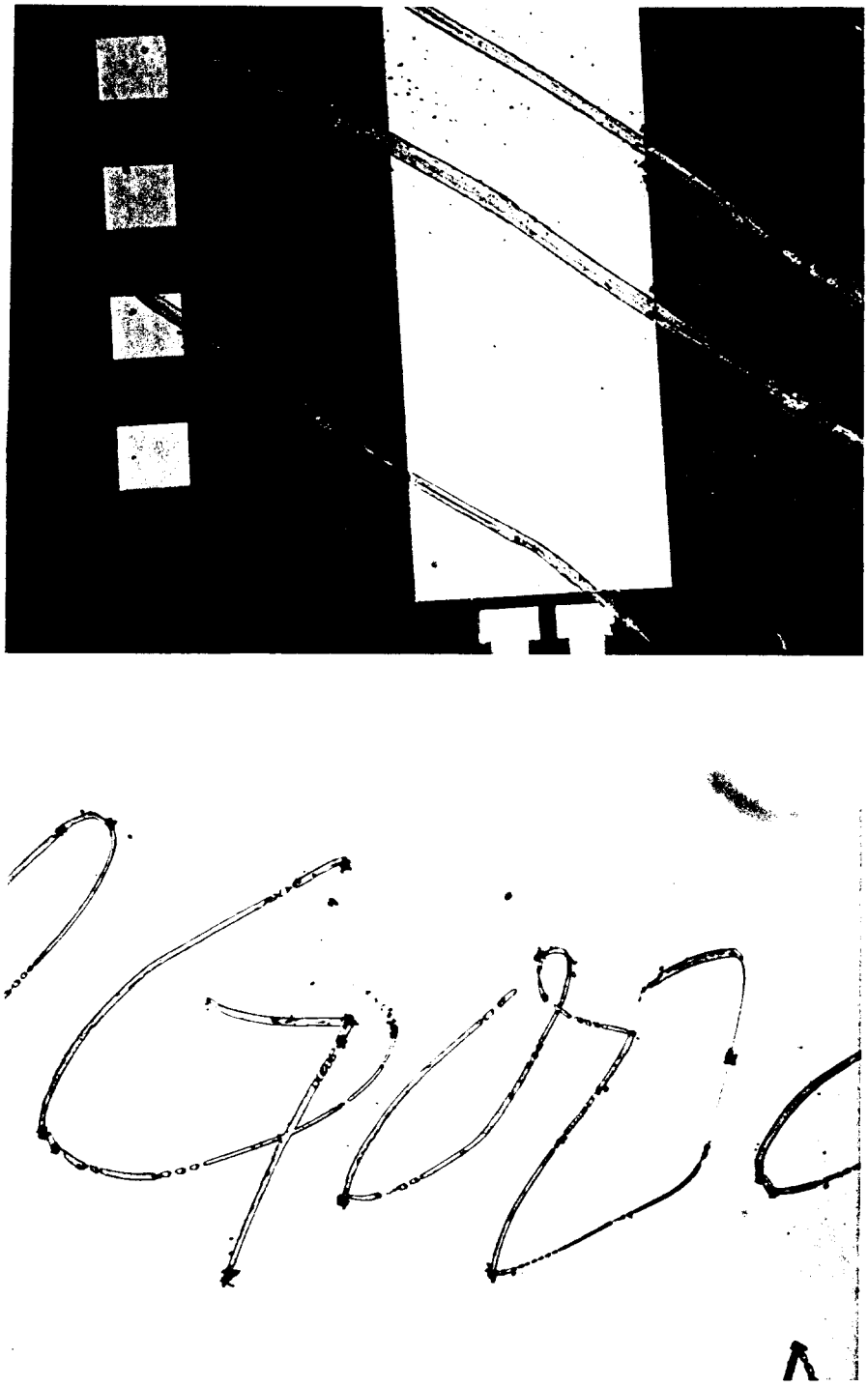

Fig. 15: Scratch tests for Ti/Ir on a thermal oxide layer; (a) with patterning (lift-off) and (b) without patterning.

Fig. 16: Metal patterns after lift-off for 50% overetched samples.

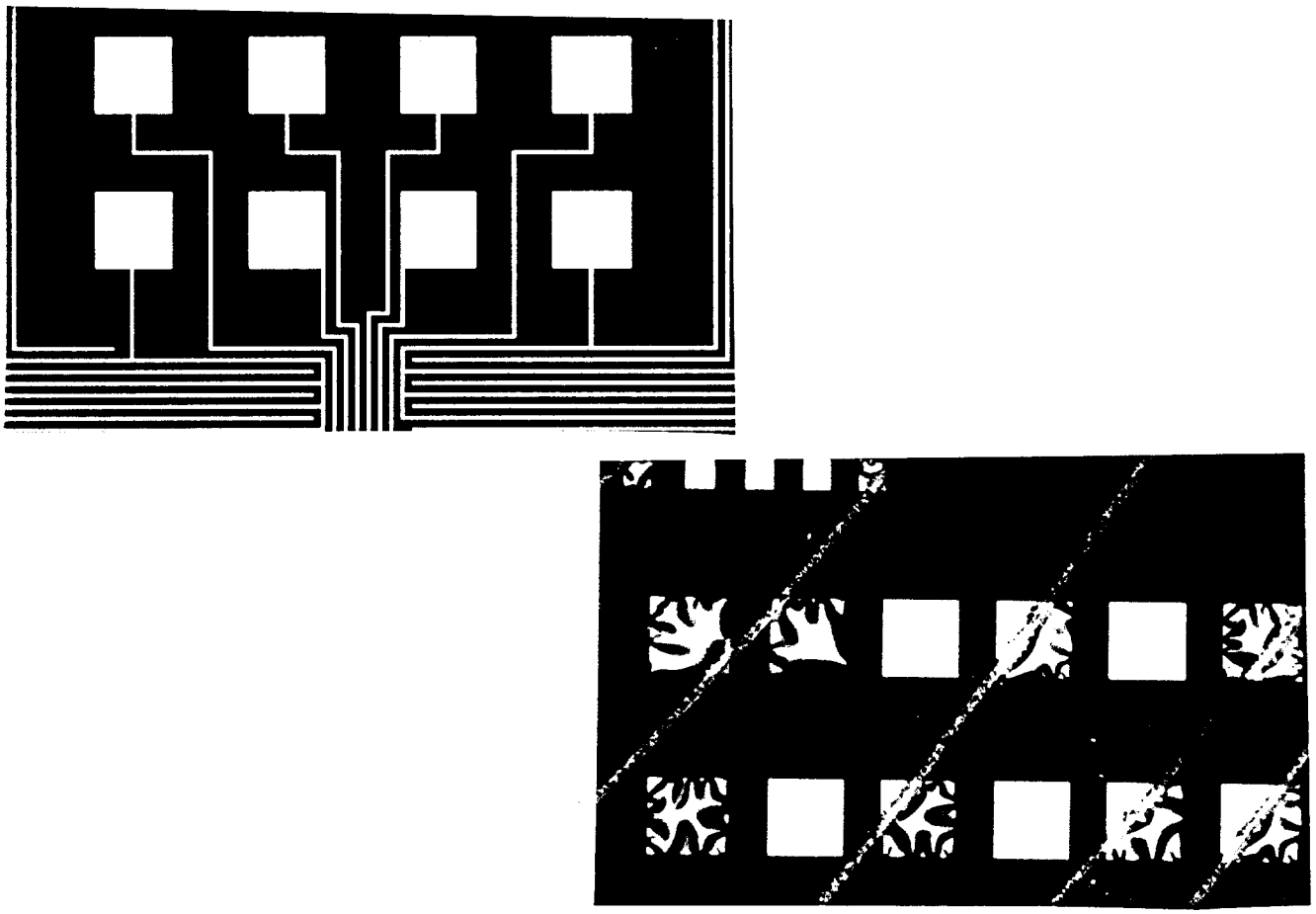

Fig. 17: Scratch test results for 10% overetched patterns. The samples look fine after lift-off but when scratched the films buckle free of the substrate, indicating poor adhesion.

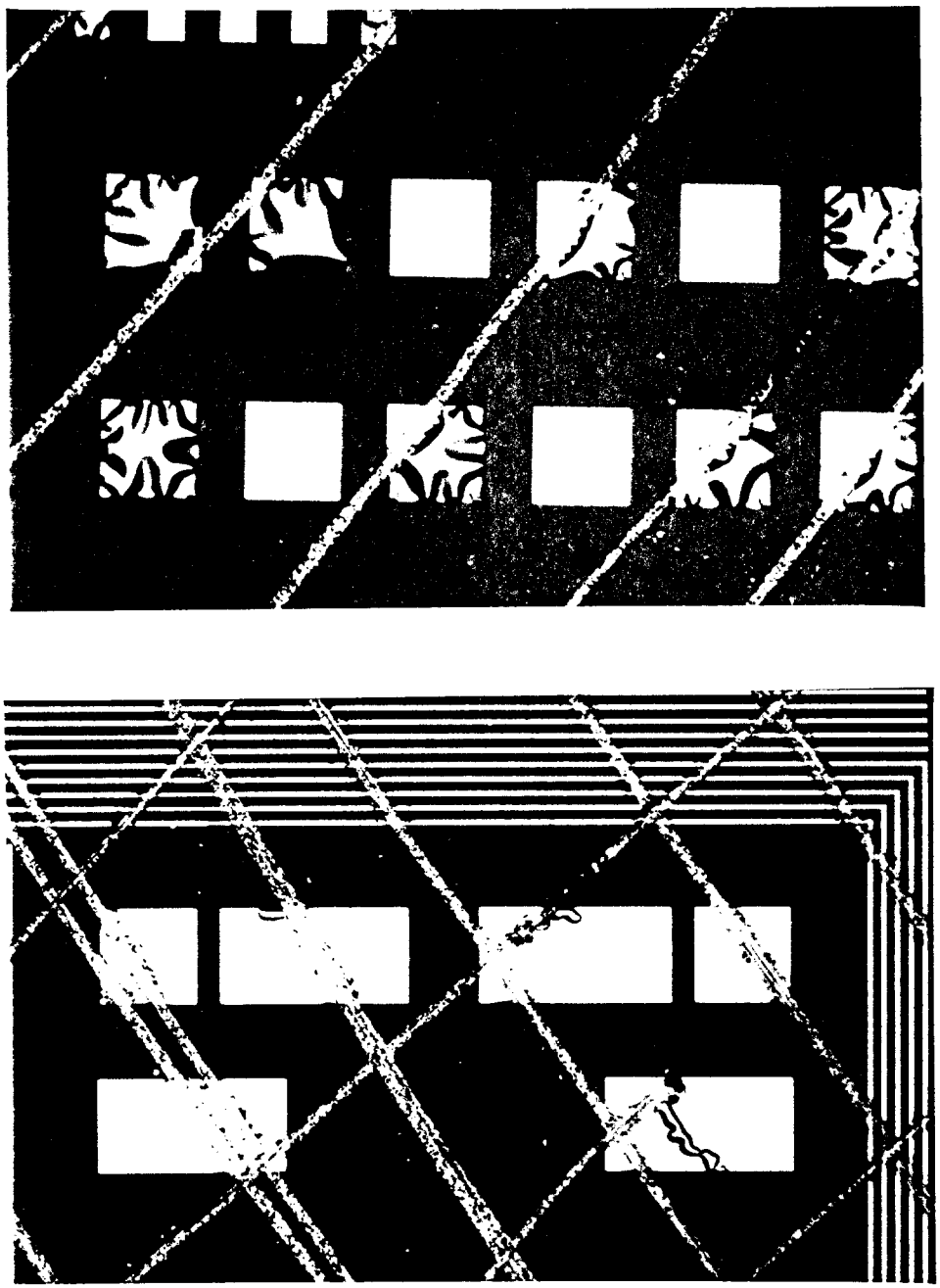

Fig 18: Scratch tests for 10% overetched samples processed wet (above) and dry (below). For wet processing, there are evident adhesion failures after scribing; the situation is much better for dry processing.

4. Rapid Thermal Annealing Tests (400-600°C, 30sec)

In an attempt to improve metal adhesion, rapid thermal annealing (RTA) tests were performed at several different temperatures ranging 400°C to 600°C in an Ar=5sccm ambient for 30sec. These samples were first annealed before lift-off in order to reduce the risk of pattern loss during the lift-off process. Lift-off was then performed to obtain the final site patterns. It was observed that higher temperatures produce better metal-to-polysilicon adhesion as shown in Fig. 19. This improvement may be due to polycide formation at the interface as a result of the surface reaction of the refractory metal (Ti) with polysilicon. Electrical tests were also performed to observe any change in contact resistance. The contact resistance dropped from 120-140Ω (nonlinear) in unannealed samples to 5.1Ω (linear) in the annealed samples as shown in Fig. 20. This test shows that RTA annealing helps both in improving adhesion and in reducing impedance.

It was found to be difficult to remove Ir metal using lift-off after RTA because of the reaction of the photoresist and metal during high thermal cycles. For this reason, we choose a second method; that is, perform the RTA after the lift-off process. A careful lift-off step is done and then RTA is performed at 500°C for 30sec in an Ar ambient. Figure 21 compares the scratch test results of samples with and without RTA at (500°C). As can be seen, the RTA process is definitely needed for good metal adhesion, and a temperature of 500°C is selected for achieving good adhesion without a metal stress problems.

Methods for Improving Site Adhesion

On the basis of these test results, the following recommendations are made for improving metal adhesion at sites and in circuit fabrication.

1. Use of an Additional Mask for Full Coverage of the Sites

As we have seen above, the metal sites are normally formed using the same mask as that used to open the dielectrics in a self-aligned lift-off process. This process has not caused any known problems to date but it does have the potential of causing problems during the EDP etching step. If the site holes are not covered completely with the iridium, then there may be an access path by which EDP can attack the underlying materials during the probe separation. In order to eliminate this chance completely, use of an additional mask for patterning the site metal is attractive so that site contact area coverage is complete and does not provide any access path for silicon etchant as shown in Fig. 22. This would increase the alignment accuracy requirements in the lithography used for recording sites since they are typically small. For stimulating sites, it should be readily accomplished. It does require that the site metal scale the sidewalls of the dielectric cuts. This site geometry will be tried during the coming quarter.

2. RTA after a Lift-Off Process

As mentioned before, use of an RTA annealing step (at 500°C, 30sec, Ar=5sccm) after lift-off is definitely recommended both for good metal adhesion and for reduction of the site impedance. This will be done routinely in all future probe fabrication.

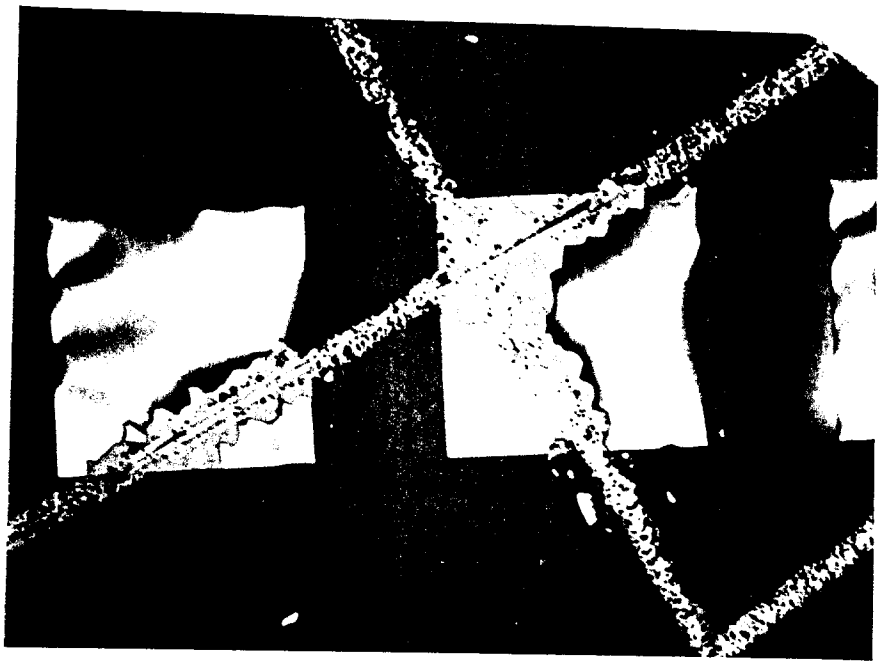

(a)

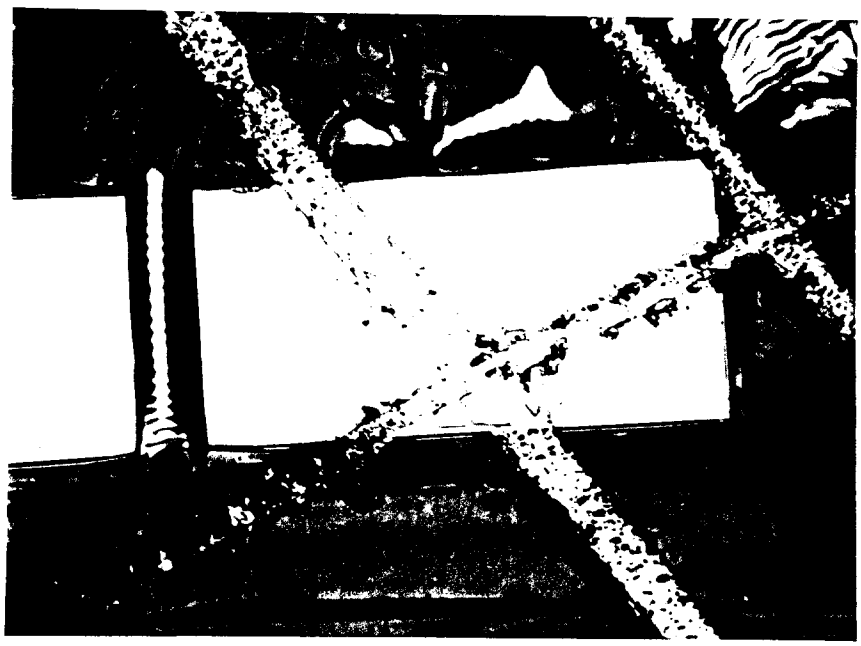

(b)

Fig. 19: RTA test results at several different temperatures; (a) original, (b) 400°C, (c) 500°C, and (d) 600°C

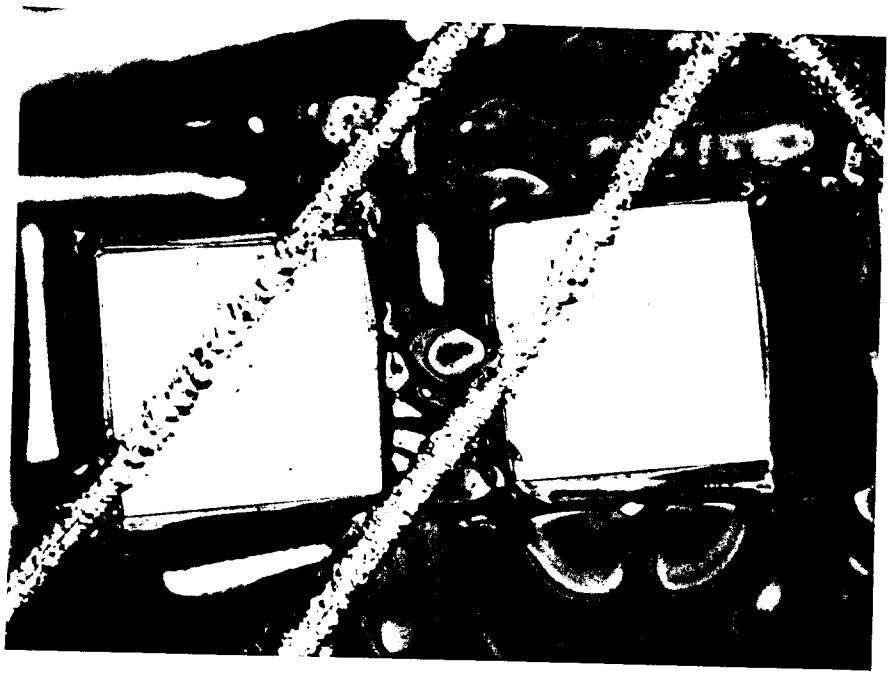

(c)

(d)

Fig. 19: RTA test results at several different temperatures; (a) original, (b) 400°C, (c) 500°C, and (d) 600°C

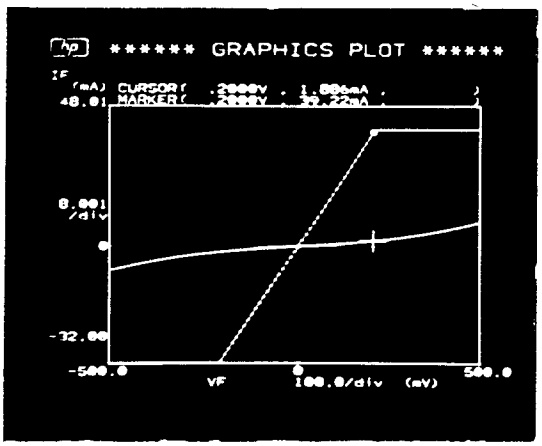

Fig. 20: Comparison of current-voltage characteristics with and without RTA (500°C, 30sec). The steep curve (low resistance) corresponds to the after RTA case.

No RTA RTA (500°C, 30 sec)

Fig. 21: Comparison of scratch test results with and without RTA.

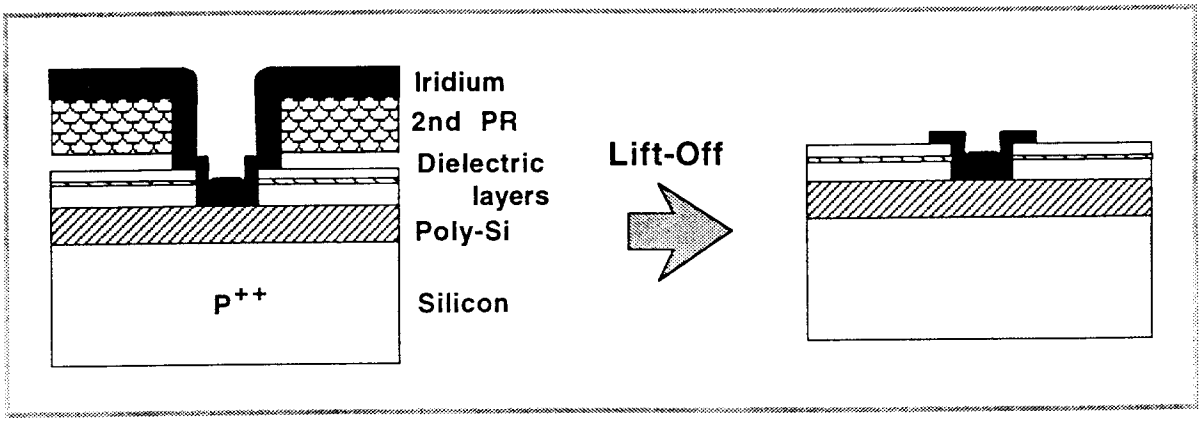

Fig. 22: Use of an additional mask for completely sealing the access path from the solution to the underlying interconnect material during probe separation in EDP.

3. Optimum RIE Etch Time

In order to minimize FC film formation during RIE, the use of an optimum etch time is very important. This can be done by monitoring the etch rate for dielectric films through regular etch characterization. It may be desireable to stop the etch early so that the final BHF etch can complete the opening of the contacts. By leaving a thin (500Å-thick) oxide layer next to the interconnect, any FC film there would be undercut and hopefully removed prior to sputtering. This will also be tried during the coming quarter.

4. Complete Sample Drying

For the complete removal of moisture from samples, the use of a spin dryer and a hot oven (110°C for 5min) are recommended to promote better metal adhesion. We also plan to install a bank of IR lamps around our sputtering system to allow some heating of the wafers during sputtering to promote more complete desorption of moisture. Heating must be limited so as not to overbake the resist, rendering it unsuitable for clean lift-off, but some heating to premote desorption is definitely desirable. Our present sputtering system has no capabilities for heating the wafers or for backsputtering, both of which would significantly help in removing moisture. Backsputtering could also remove surface FC films. A new sputtering system that can be dedicated to probe fabrication is high on our wish list of equipment and will be a target for acquisition during the coming year.

6. Development of Active Stimulating Probes

During the past quarter, we fabricated another run of active stimulating probes using the off-tilt alignment method (10°~20°) to solve the excessive corner undercutting problem reported in Quarterly Report #4. The time schedule was delayed for two months because of the lack of availability of laboratory equipment. (In particular, our tube for nitride-oxide deposition was down. We have recently received a grant from NSF to allow

replacement of the pumps and particle trapping on this system as well as the installation of an LTO/PSG system for probe fabrication. These equipment upgrades should be completed by early next year.) The active circuitry was encapsulated with a 1μm thick layer of LTO (low temperature oxide, 420°C), which was thick enough to protect the CMOS circuitry in EDP during probe separation (at 110°C for 2.5hrs). We tested the stimulating probes just before final micromachining to rule out all process related problems. All circuits were working and test results were very encouraging. Following final etching in EDP, the active probes were visually inspected and mounted on PC boards. At this point they were ready for final testing.

TEST RESULTS

DC Device Characteristics

Figure 23 shows the current-voltage characteristics for W/L=30/3μm CMOS devices which have reasonable current drive capability, with threshold voltages of 0.9V and -1.0V for the n-MOS and p-MOS devices, respectively. The use of wide p-well separation and a thick n-epi layer has helped significantly in reducing the standby current (from a few tens of mA in STIM-1). Figure 24 shows the supply current characteristics versus power supply voltage, V_{cc}, in STIM-2 for two different samples. A power supply current of about 50μA was measured at V_{cc}=5V. This result demonstrates that low power electronics are possible in this application with this design.

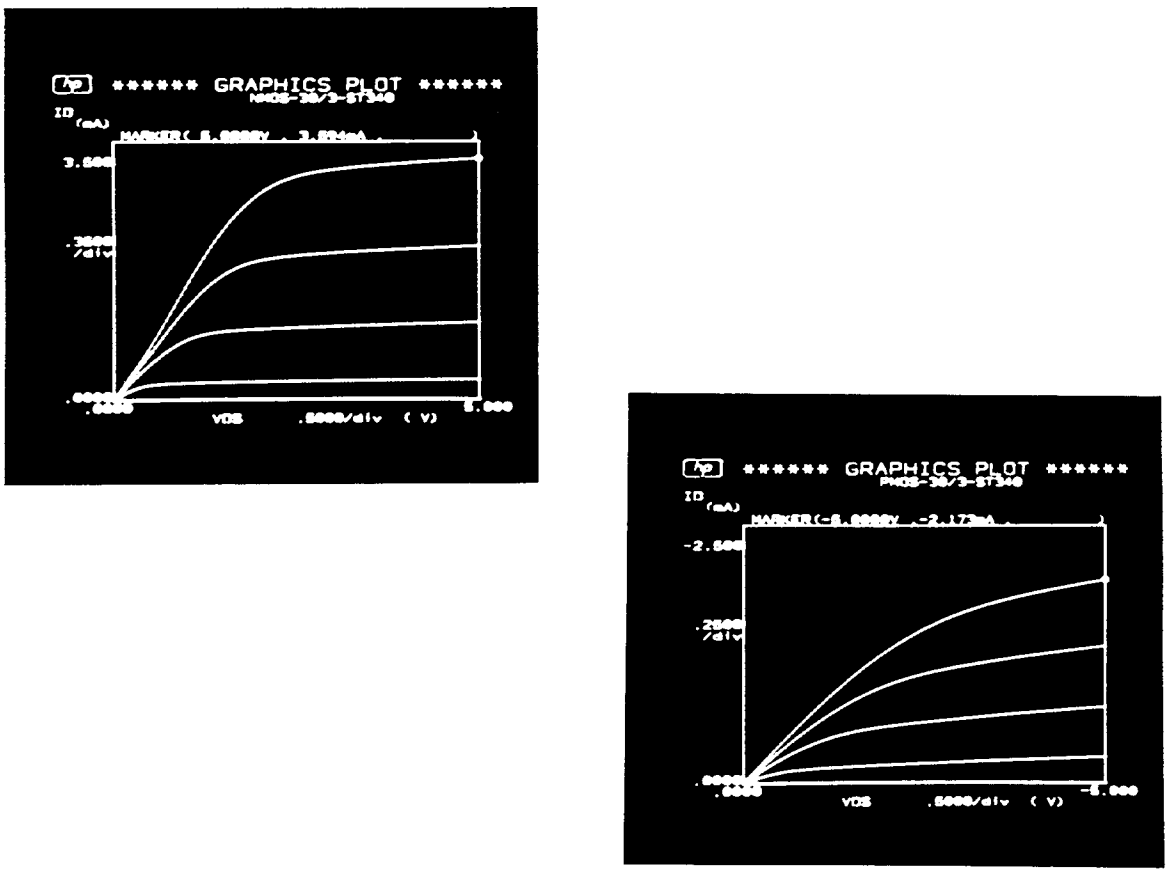

Fig. 23: Current-voltage characteristics for W/L=30/3μm CMOS devices after final thermal cycles. The n-MOS device is shown above with the p-MOS device below.

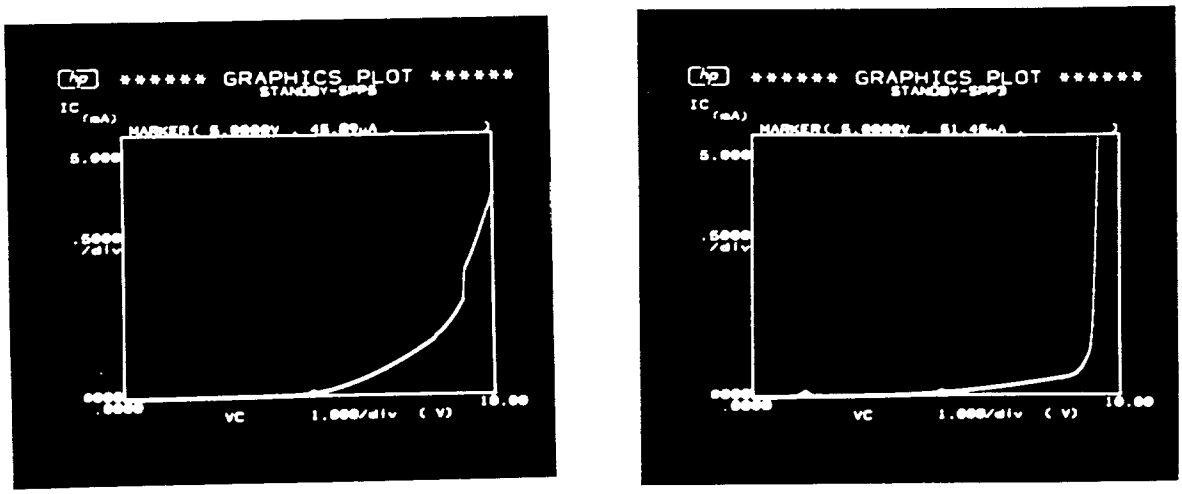

Fig. 24: Power supply current (I_{cc}) characteristics with various power supply voltage, V_{cc}, for two different probes. The leakage currents are 46μA and 51μA at 5V, but the increase in current above 5V is much steeper in the one device than in the other. STIM-2 is designed to run at 5V, where this amount of background current is acceptable.

Test Results after EDP

In this run, we coated working STIM probes with thick LTO (1μm) and then etched the probes in EDP for 2.5hrs in order to separate the probes from their wafers. Figure 25 shows the etched profile of the back area of a probe displaying full coverage of the CMOS circuit area onwith a 110μm-thick substrate. Figure 26 shows an SEM photograph of the surface topography of one of the LTO-coated CMOS circuits after EDP. The step coverage appears to be excellent and no attack of the circuitry by EDP can be found. Figure 27 shows one of the probe tips on STIM-2. The very sharp edges on these shanks is characteristic of the profiles produced by the shallow boron diffusion combined with a deep boron-diffused etch-stop. Figure 28 shows examples of the etched STIM-2 probes. The full set is shown: STIM-1b (monopolar), STIM-1a (bipolar), and STIM-2 (multipolar).

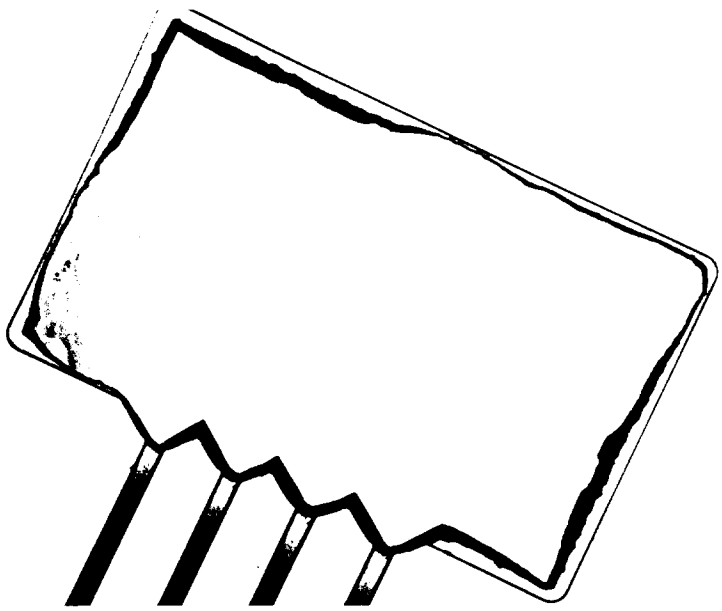

Fig. 25: Etched profile of the rear portion of an active probe showing full coverage of the CMOS circuit area with a 110μm-thick substrate.

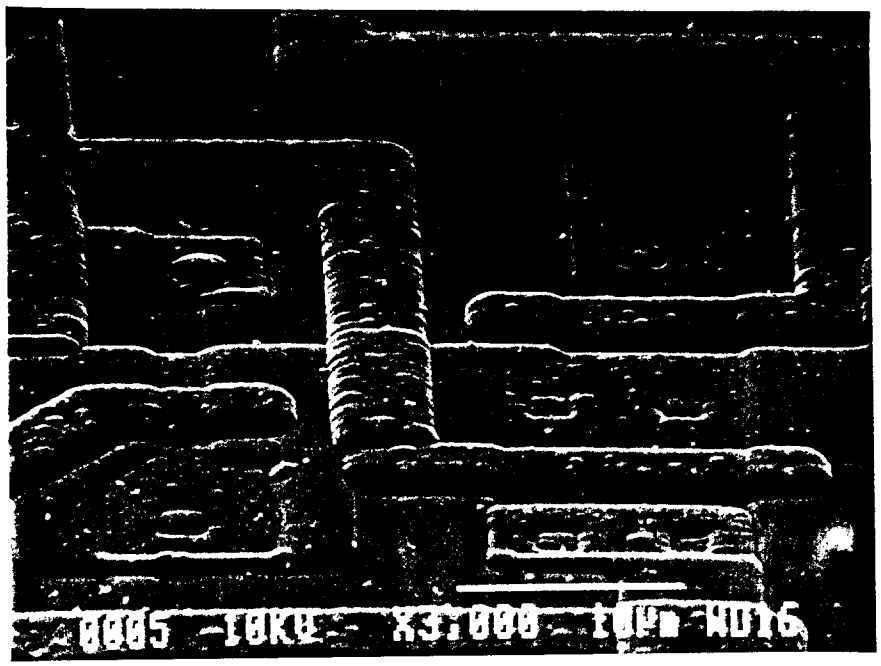

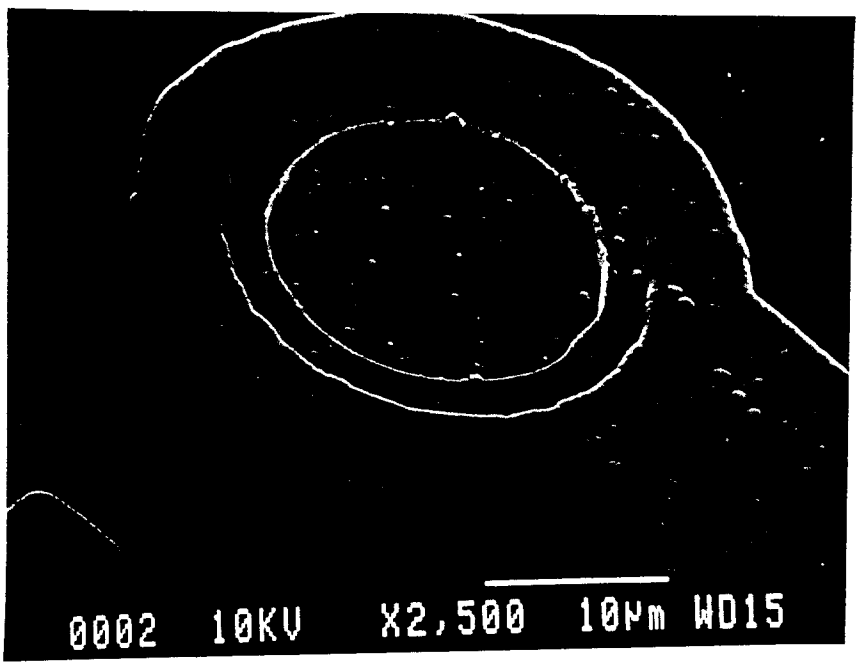

Fig. 26: SEM photograph of the surface topography on one of the LTO-coated CMOS circuit areas after EDP. An iridium stimulating site is also shown.

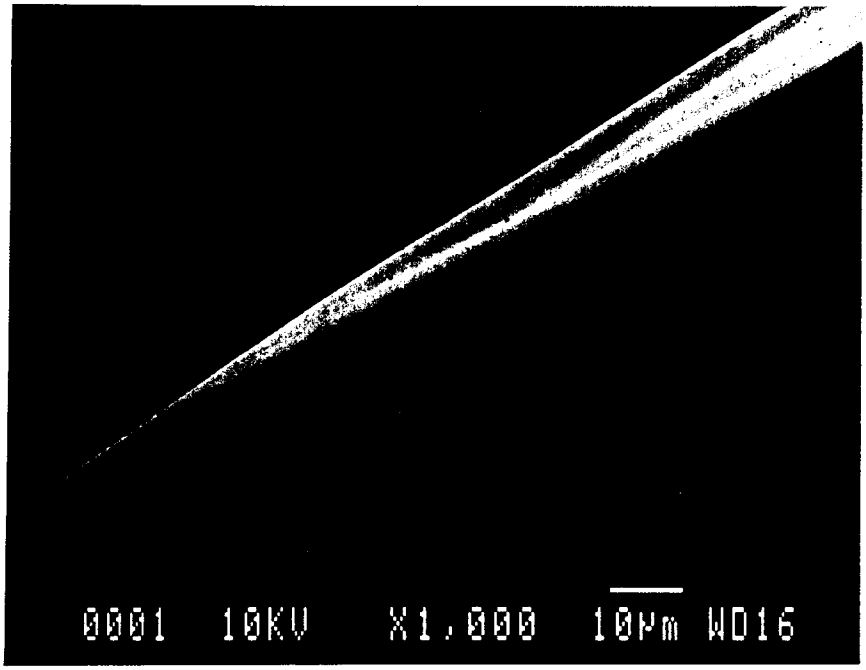

Fig. 27: One of the shank tips on STIM-2, formed with a shallow boron diffusion extension of the deep boron diffusion that defines the main portion of the shank.

PROBE CIRCUIT TEST RESULTS

STIM-1B

STIM-1B is the monopolar version of the stimulating probes. In this case, site address information is entered serially using the clock to increment an on-chip counter. The counter state is decoded to select the desired site, which receives the externally-generated current via an on-chip analog multiplexer. Figure 29 shows the operation of the monopolar probe. The upper trace is the input clock signal, which is used to set the site address. The address here is set first at site #1 and is then switched to site #4. The middle trace shows the site-drive signal, which in this case is an arbitrary waveform used for illustration only. The bottom trace shows the measured voltage output waveform at site #1 across a 10kΩ resistor. Site #1 receives input only when addressed.

STIM-1A

STIM-1A is a medium-complexity version of the active stimulating probes which is used for a bipolar stimulation. To effectively stimulate the tissue, a bipolar current drive scheme is adopted; both current sourcing and sinking operations are simultaneously possible on the sites during the stimulating active cycle. This concept, which is based on charge balance, effectively stimulates tissue while reducing tissue damage and improving probe reliability. In the bipolar case, eight bits of serial data are used to select two sites. The subsequent 8 bits of current amplitude data are then used on-chip to generate the stimulus current for the first site using a current-output digital-to-analog converter (DAC). This current is mirrored to the second site to form a bipolar pair. Figure 30 shows the operation of the bipolar probe. The upper two traces is the 16-state serial input clock signal, which is used to control the shift register to accept external data information. The center trace shows the site-drive data signal (address and current level). The address here is alternatively set at site #4 to generate 4 combination patterns (1111111, 0111111,

0011111, and 0001111) for both sinking current and sourcing current. The bottom trace shows the measured voltage output waveform at site #4 across a 10kΩ resistor. Site #4 properly provides both sourcing current and sinking current alternately when addressed.

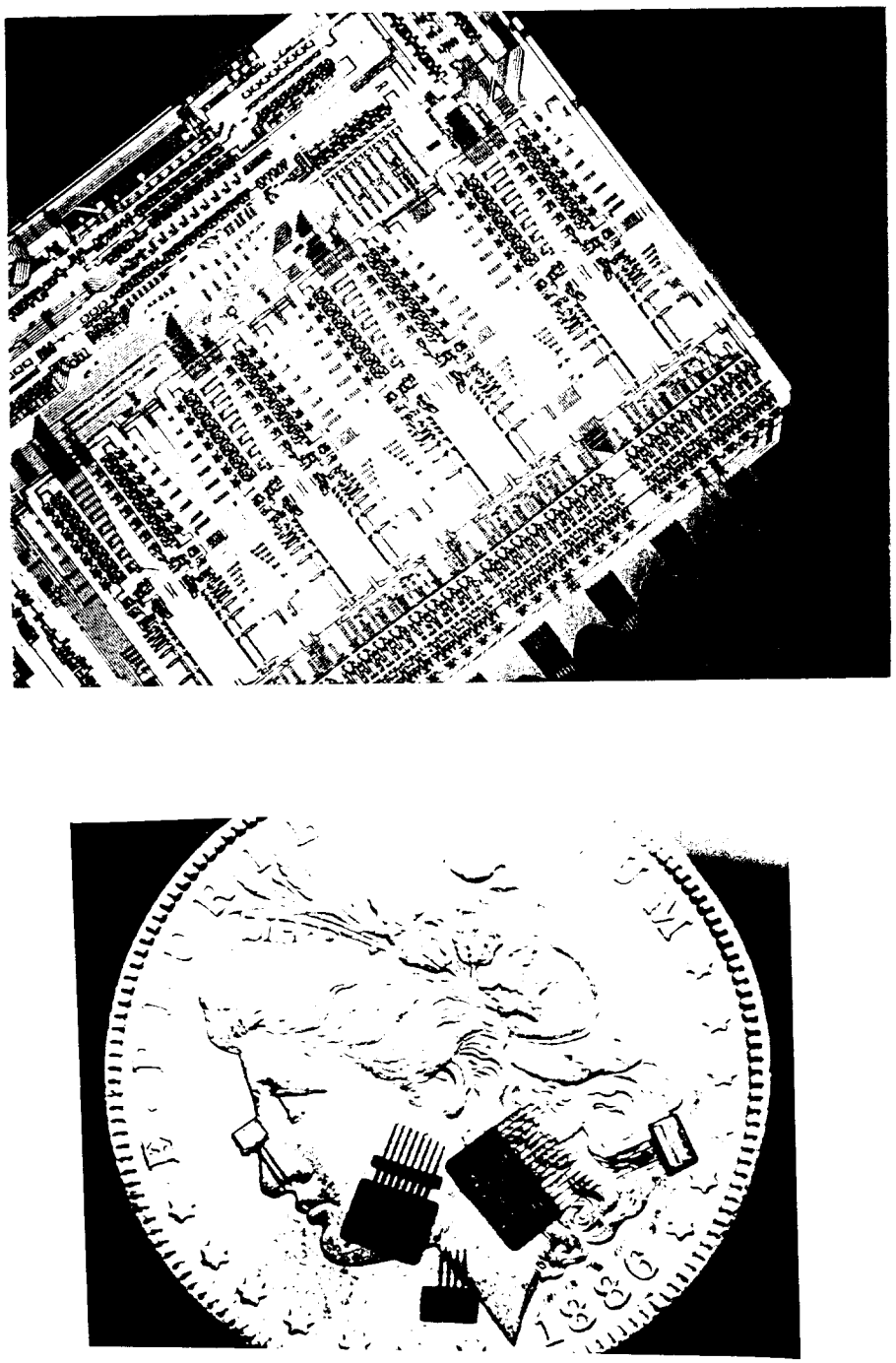

Fig. 28: Examples of the etched family of second-generation active stimulating probes: STIM-1a; STIM-1b; and STIM-2.

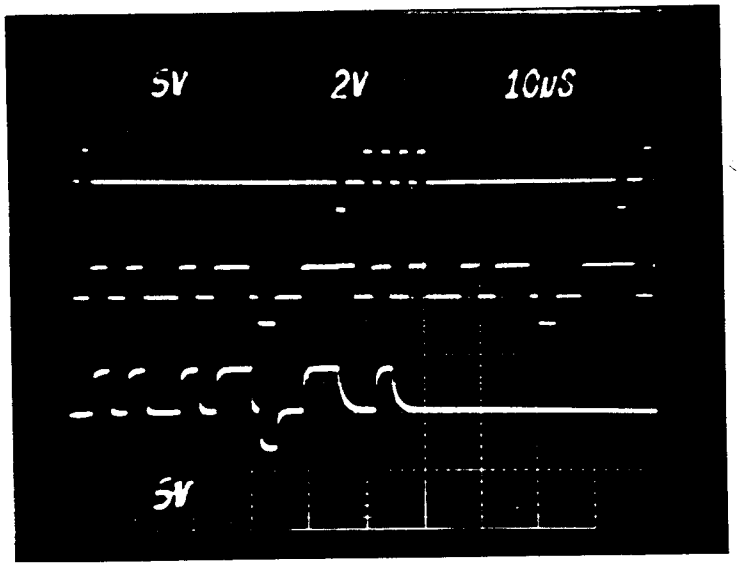

Fig. 29: Operation of the monopolar probe. Upper trace: input clock signal; middle trace: site-drive signal; bottom trace: measured voltage output waveform across a 10kΩ resistor. Site #1 receives input only when addressed.

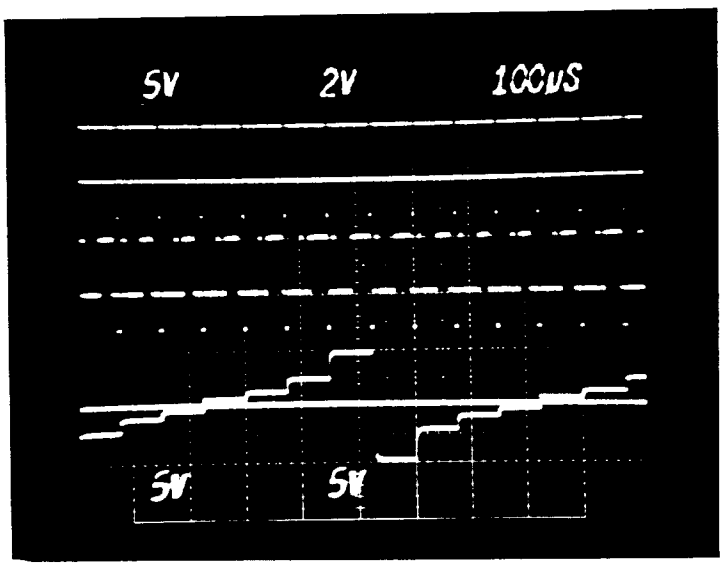

Fig. 30: Operation of the bipolar probe. The top trace is the 16-cycle input clock and the middle trace is the input address and current level data. In this case, site #4 is selected and several different current levels are provided, both sourcing and sinking, alternating four combinations (1111111, 0111111, 0011111, and 0001111). The bottom trace shows the measured voltage output waveform at site #4 across a 10kΩ resistor.

STIM-2

STIM-2 is a second-generation probe that significantly extends the first-generation design in a number of areas: 1) flexible interconnects, fabricated as part of the chip, allow the rear portion of the circuit area to be folded flat against the cortical surface to reduce the probe height above the cortex to <1mm, which results in a low-profile probe; 2) the probe offers a variety of new circuit designs to reduce power and circuit area while increasing functionality; 3) a front-end channel selector allows any 8 of the 64 sites to be driven simultaneously, effectively implementing electronic site positioning; and 4) the probe is directly compatible with use in multi-probe three-dimensional arrays, initially targeted at 256 shanks and 1024 sites. The addressed per-channel data latches lock onto the data when the clock line is strobed negatively and the DAC generates the appropriate currents. Figure 31 shows output voltage waveforms across a 20kΩ resistor load when the current level data alternate from (1111111) to (0000111) (16 combinations) for a sourcing case (CP=1).

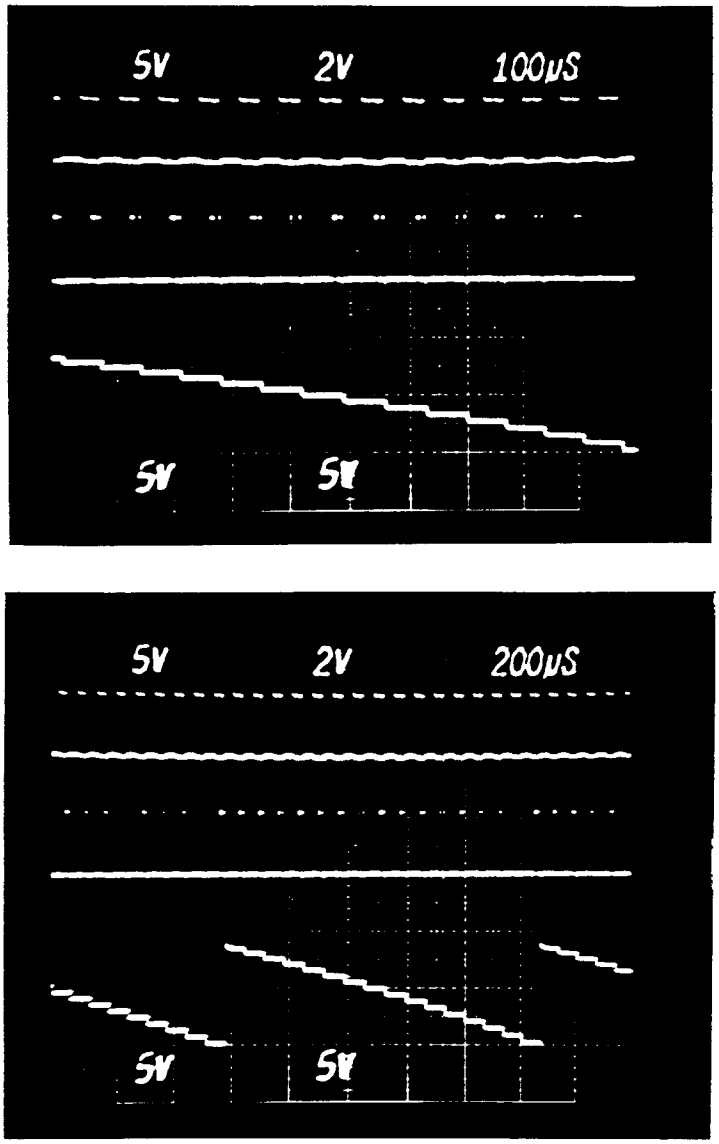

Fig. 31: Output voltage waveforms across a 20kΩ resistor load when the current level data alternate from (1111111) to (0000111) for the sourcing case (CP=1).

We believe all versions of the active stimulating probes are working correctly. During the next quarter, we anticipate more thorough testing in vitro using the computer-driven external interface electronics. Following these tests, we will proceed to in-vivo testing. Long looked for, come at last.

6. *External Electronics for Active Stimulation Probes*

In the previous quarter, the hardware development for the remote converter was completed. Together with the PC daughterboard, a functional system now exists for controlling the active stimulation probes. The daughterboard was debugged and tested with MOSIS STIM-1 and STIM-2 chips. Integration and testing with actual STIM-2 probes will begin during the coming quarter now that these devices are available.

The focus of the control system development has now shifted to interface software. The original software that was used to perform low-level testing was sufficient for this purpose but was judged too rudimentary for higher-level testing. This software has been replaced with a more flexible system that includes a programmable interpreter with a built-in scripting language. This new system allows for rapid prototyping and repeatable testing under program control.

The next phase of software development will concentrate on adding functionality to the software executing on the Chimera board. This board acts as the support and PC interface to the daughterboard hardware. Currently, the software executing on the Chimera board acts only as a gateway for data between the PC and the daughterboard. Eventually, the waveforms that are to be generated by the probe will grow more complex and the PC-to-daughterboard interface will prove too slow to support complex waveforms. The Chimera software will address this problem by generating the waveform data directly while accepting only parameter information from the PC at a much lower data rate.

7. *Conclusions*

During the past quarter, research under this program has focused in several areas. We have continued to produce a variety of passive stimulating probes and provide them to internal and external users. Additional experiments have been performed in penetrating the pia and dura with both single-shank and ten-shank probe structures. Both probes with shallow-diffused (sharp, 10°) tips and probes with deep-diffused (blunt, 45°) tips penetrate the pia mater with little discernable cortical dimpling. The cortical depression using these tips with an insertion rate of 1mm/sec is estimated at about 250μm and 800μm, respectively. The force on the probe shanks is in about the same ratio for these two tip designs. New interface electronics for the on-chip strain gauges now allows ample force resolution, but breathing and cardiovascular artifacts remain a problem. None of these probes have successfully penetrated dura mater since their present thicknesses (14μm) reduce their stiffness and allow them to buckle excessively before penetration. During the coming term we hope to extend these measurements to eliminate some of the artifacts and to explore the effects of insertion rate on force and cortical dimpling. It is noteworthy that using the sharp tips, we see virtually no bleeding even when intentionally penetrating surface vessels. The insertion holes are evidently self-sealing, both with the probe in place and when they are removed.

Experiments to evaluate tissue reaction to stimulation continued during the quarter. Using charge-balanced anodic-first 50μA current pulses with 100μsec per phase, anodic

bias (0.6V) on the site was found to significantly reduce back-voltage. SEM inspection of sites on a probe implanted and stimulated for five days, and then sacrificed four weeks later, showed tissue adhering to all sites that were stimulated. No site that was inactive (not used for stimulation) had any appreciable tissue growth over it. Most sites that were stimulated had an overlay of tissue on them, sometimes relatively thick in appearance. Tests to further understand and quantify these effects are continuing.

A new computer-controlled system for site activation, deactivation, and cyclic voltammetry is also being developed using LabVIEW. The system will offer the user control over a variety of parameters, will ensure reproducibility in the activation process, and will require minimal user interactions during the activation process. This system is now nearing completion.

We believe the iridium adhesion problems we have been experiencing for the past three years are now understood and can be eliminated from future runs. The problems have been traced primarily to the RIE dielectric etch step which precedes metal deposition. This step has been depositing fluorocarbon films ("teflon") on the sites which acts as an electrical impedance barrier and degrades adhesion of the titanium metal, deposited as a glue under the iridium. Secondarily, moisture is a problem degrading adhesion. We have found that minimization of RIE overetch, increasing the titanium thickness to ensure adequate coverage over all of the site, use of a dehydration bake prior to metallization, and use of a 500°C 30sec rapid thermal anneal after lift-off can eliminate these adhesion problems.

A new run of active stimulating probes has been completed. A full set of second-generation active probes (STIM-1b, STIM-1a, and STIM-2) has been realized. All of these probes appear to be functioning adequately. Detailed in-vitro and in-vivo tests should begin during the coming quarter.